Atomization and Sprays, vol. 17, pp. 551–568, 2007

TRANSITIONAL INSTABILITY OF A PRESSURE-SWIRL ATOMIZER DUE TO AIR-CORE ERUPTION AT LOW TEMPERATURE

Byung-Sung Park
Desalination Plant BG, Middle East R&D Center,
Doosan Heavy Industries & Construction. Co. Ltd.

Ho Young Kim* and Sam S. Yoon
Department of Mechanical Engineering, Korea University, Anamdong,
5-Ga, Sungbukgu, Seoul, 136-701, Korea

Original Manuscript Submitted: 4/3/06; Final Draft Received: 7/12/06

Because of the high viscosity of fuel in low-temperature environments, jet fuel in a pressure-swirl (or simplex) atomizer undergoes a transitional stage in which an unstable mode of the jet is found. This transitional instability at low fuel temperature is observed not only at an external location, where the pulsation of a hollow cone is visualized, but also inside the atomizer, where measurement of the flow's inlet pressure and flow rate takes place. The breakdown of an air core (formed due to high centrifugal acceleration inside the swirling atomizer) may explain the instability. When the jet is stable at high temperature, a hollow cone is formed and the mass flow-rate distribution forms a hump at the spray collection plate, at the downward location. When the fuel temperature is decreased, the hollow-cone spray becomes a solid-cone spray, due to the disappearance of the air core inside the atomizer, in which case turbulence begins to dominate. The objective of the current work is to measure the effect of liquid temperature and viscosity on the atomization behavior of a pressure-swirl nozzle. In the experiment, kerosene-based aviation fuels (referred to as Fuel A and Fuel B) are the working fluids. The inner diameter of the orifice at the fluid exiting location is 1 mm. The ranges for the operating pressure and fuel temperature are 0.2 MPa < P < 1.0 MPa and 253 K < T < 313 K, respectively.

INTRODUCTION

Pressure-swirl (or simplex) atomizers are used in many industrial applications, such as aircraft turbine engines, air conditioners, sprinklers, and fire

*Corresponding author; e-mail: kimhy@korea.ac.kr

suppression. In particular, pressure swirl is widely used in aircraft internal combustion (IC) engines because of its high atomization performance and its reliable deterrence against combustion instability.

A hole that allows a tangential entry of liquid into the cylindrical swirl chamber is shown in Fig. 1a, to depict a typical internal geometry of a pressure-swirl atomizer. The tangential velocity of the liquid is further increased through the converging conical cylinder, while its angular momentum is maintained. This high tangential velocity is transformed into radial velocity when liquid exits the orifice plane. Since the cone angle, θ, of the spray is defined by the ratio of the radial and axial velocities of the liquid, the cone angle of a pressure-swirl atomizer is generally high; an extreme case is $\theta = 180^{o}$. Due to the high centrifugal force within the swirl chamber of the atomizer, an air core is formed whose cross-sectional center area is occupied by air. As a result, the discharge coefficient ($C_d = \dot{Q}_{\text{actual}}/\dot{Q}_{\text{theory}}$) of any pressure-swirl atomizer is always less than unity.

Inviscid analyses have been applied to analyze the pressure-swirl atomizer. Taylor [1] is probably the first investigator who showed that the bulk motion of the fluid could be described by potential flow theory. Giffen and Muraszew [2] predicted the air-core diameter using the inviscid theory of the maximum flow principle, implying that the air-core diameter will adjust so that the mass flow rate reaches its peak value. The work of Giffen and Muraszew [2] has been followed by Dombrowski and Hassan [3], Clark and Dombrowski [4], and Rizk and Lefebvre [5], all of which noted that the inviscid analysis provided a basic understanding of the characteristics of pressure-swirl atomizers. More recently, the state-of-the-art quasi-3D simulation for a swirling jet was performed using the potential flow theory [6]. Lefebvre [7] also noted that the discharge coefficient, a measure for the ratio of air-core diameter to orifice diameter, is independent of Reynolds numbers greater than approximately 3000. However, Taylor [8] later pointed out that the boundary layer effect dominated in the film thickness of the exiting liquid and other related parameters, such as droplet size. The discharge coefficient is also known to vary when the liquid viscosity changes [9].

Kim et al. [10] reported on the boundary layer effects of swirl atomizers; their work can be summarized as follows. (1) When the tangential entry port area increases under the constant orifice exit area, the discharge coefficient increases, which indicates a decrease in the air-core diameter. (2) When the operating pressure increases, the film thickness decreases (indicating an increase in the air core diameter). (3) When the orifice length increases, swirling intensity is reduced and the cone angle therefore also reduces; but the breakup length increases because of the increase in the

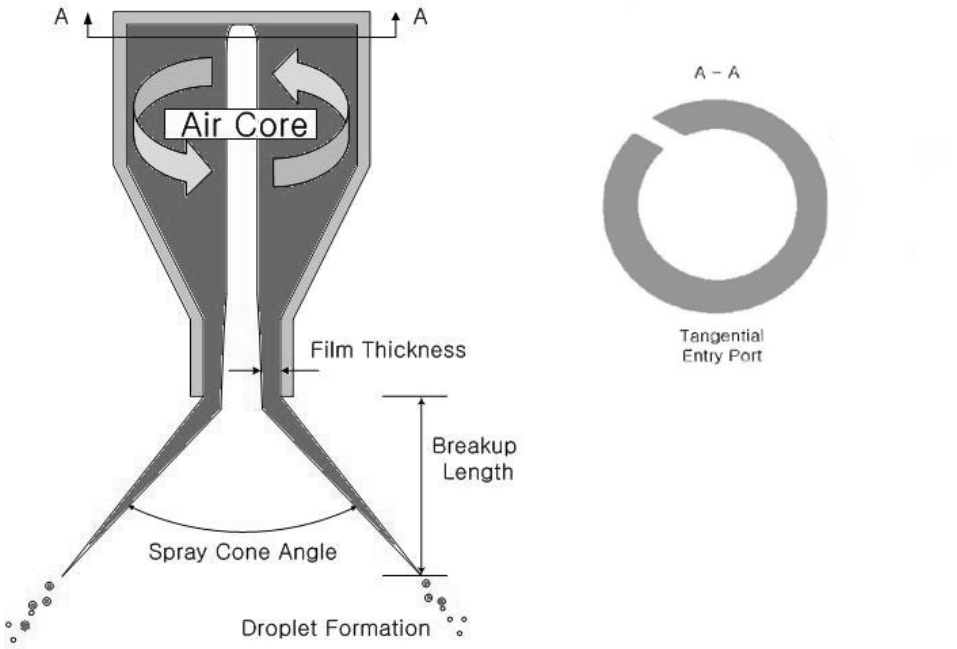

a)

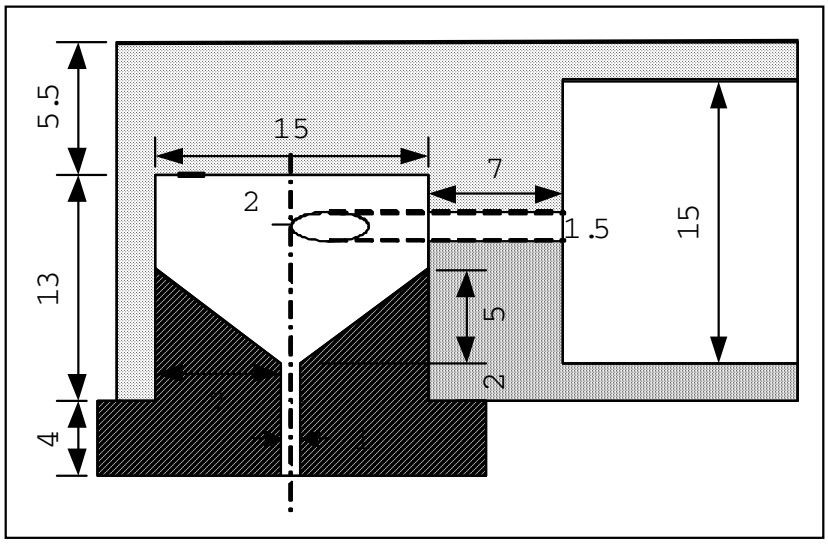

b)

Fig. 1 (a) Schematic of a typical pressure-swirl atomizer and (b) The internal geometry of the pressure swirl used for the current study. All dimensions are in millimeters.

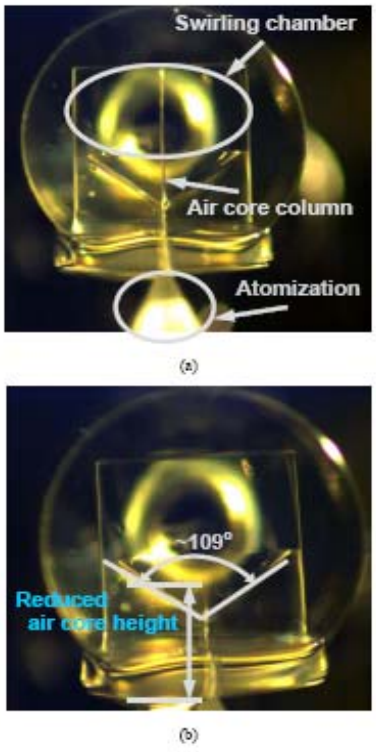

Fig. 2 Reduction of the air-core column height of the swirl atomizer when the temperature is reduced from (a) 40^{o}C to (b) 20^{o}C. The air core eventually disappears due to the increase in the fuel's viscosity at the low temperature.

boundary layer thickness, which generally requires a longer time for the roll-up motion to appear.

Despite these studies, the effect of liquid temperature on the characteristics of pressure-swirl atomizers has not yet been fully explored. Certain aircraft engine fuels (referred to here as kerosene-based "Fuel A" and "Fuel B") undergo a transitional stage when their temperature changes due to the eruption of the swirling air core at lower temperatures (or higher viscosity). When the swirl is weak (whether due to the high viscosity of the fuel at low temperatures or because of low injection pressure), the air core breaks up and eventually disappears. (See Fig. 2 for development of the air core disappearance.) During this transitional process, the entire jet pulsates and becomes unstable. This phenomenon causes problems in the aircraft engine because the development of the combustion occurs during the pulsation, when the engine is exposed to a cold environment.

The droplet size and liquid volume distributions of the considered pressure-swirl atomizer-as well as the effects of the transitional behavior on the discharge coefficient-are reported here. Recommendations are made to improve the quality of the design for the pressure-swirl atomizer while circumventing the operational limitations associated with cold weather.

EXPERIMENTAL SETUP

Pressure-Swirl Atomizer

The schematic for the internal geometry of the pressure-swirl atomizer used in this experiment is shown in Fig. 1b. The container of fuel (see the fuel tank whose size is 15 mm in height in Fig. 1b) was pressurized and the fuel entered through the tangential port into the swirl chamber, whose diameter was also 15 mm, as indicated in Fig. 1b. Remember that there was only one tangential entry port in our atomizer; thus, the swirling strength was relatively low when compared with other multiport pressure-swirl atomizers. While the swirling strength was generated inside the swirling chamber, the fuel traveled downstream in a helical manner, similar to that of a hurricane. Because of the swirl's high centrifugal force, a void column, known as the air core, was formed at the atomizer's center, which is typical of a pressure-swirl atomizer. This air-core formation is manifest in Fig. 2a of our experiment. The converging angle of the conically shaped part of the swirling chamber was approximately 109^{o} (see Fig. 2b), and was followed by a constant-diameter section of length 6 mm.

Experimental Apparatus

The schematic diagram of the experimental apparatus is shown in Fig. 3. Fuel pressurized by nitrogen gas in the tank was provided through the heat exchanger, submerged in a bath, which controlled the fuel temperature. The temperature-controlled fuel was supplied to the atomizer. A pressure transducer and thermocouples were installed in the fuel supply pipe, located between the heat exchanger and the atomizer, to measure the injection (or operating) pressure and the fuel temperature, whose uncertainties lie within 1% error, according to the manufacturer's manual. The volumetric (or mass) flow rate was measured using a gear displacement flow meter, whose accuracy lies within 1% error.

A Malvern particle sizer measured the SMD (Sauter mean diameter), using the Fraunhofer diffraction of a parallel beam of monochromatic light by the moving droplets. The Malvern particle sizer was installed downstream

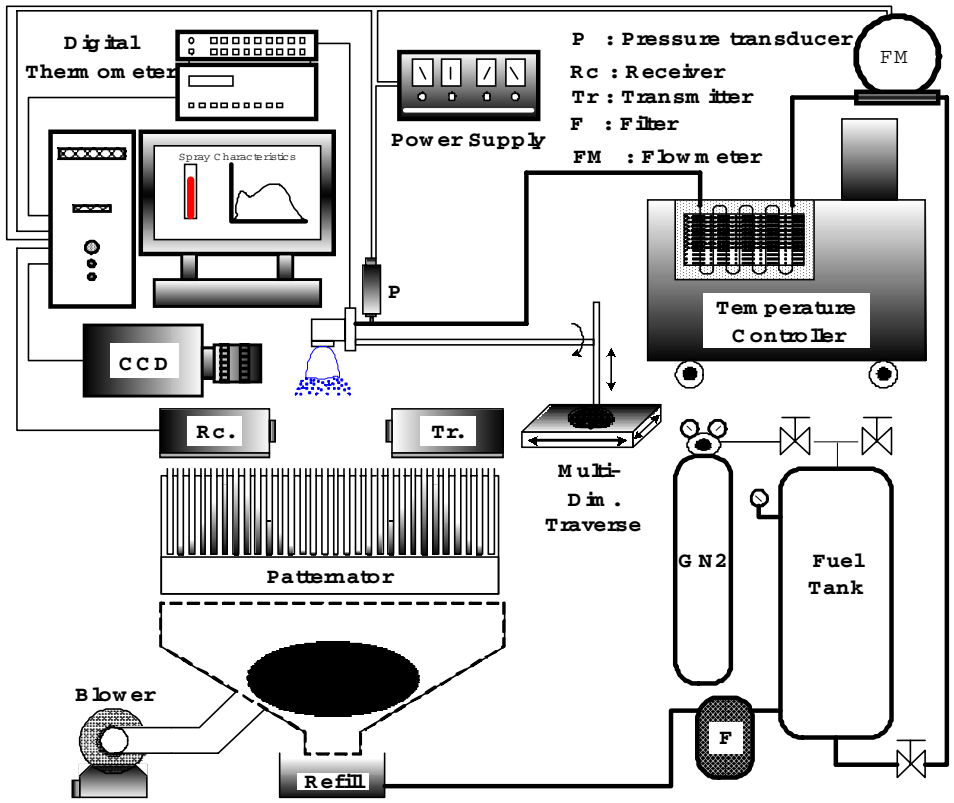

Fig. 3 Schematic of the experimental setup.

of the atomizer's tip, while analyzing the diffraction pattern produced by a continuous laser beam passing through the atomized droplets at downstream locations. The Rosin–Rammler distribution was utilized to fit the data collected downstream. Three modules comprised the Malvern particle sizer: a transmitter, a receiver, and a computer. The transmitter included a 5 mW He–Ne laser emitted as an optical beam column; a 9 mm beam expander and a 300 mm lens were used. The receiver contained a lens, detector, associated electronics, and computer interfaces. The size of the atomized droplets ranged from 5 to 500 μm, whose estimated uncertainty lies within ±5% error according to previous experience [8]. The detector monitored an average value of the light-scattering characteristics whose values were based on statistically reliable data sets, i.e., several million droplets.

The spray cone angle was measured at 3 cm downstream from the atomizer tip using the spray images captured from the CCD camera, located about 1.2 m from the nozzle. The camera resolution ranged from 500 to

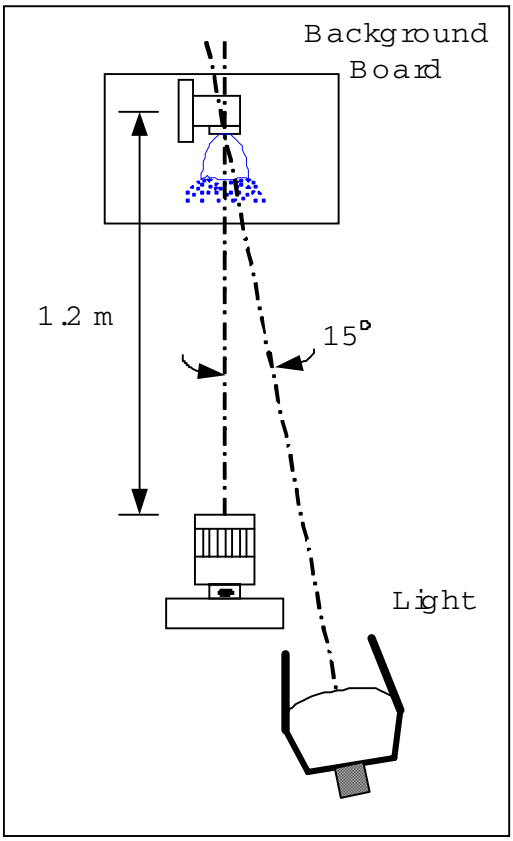

Fig. 4 Schematic of the experimental setup, which shows the orientation of the CCD camera capturing the injecting spray.

100,000 fps (frames per second). The front-lighting technique was used with 1 kW illumination power. The light was projected with a slightly oblique angle of 15^{o}, as shown in Fig. 4. The images obtained from the camera were transferred to a data processing computer and used to measure the spray-cone angle. A stroboscope illuminated the visualization of the spray's dispersed pattern. The volume distribution of the atomizer was measured by a 1D patternator, consisting of 30 collecting bins connected to a refilling container that recycled the collected fuel through the closed-loop fuel tank system.

Fuel Properties

The fuels used for the current study are the kerosene-based aviation fuels used in an aircraft turbine engine (hereafter referred to as "Fuel A" and "Fuel B"). Even though fuel formulas cannot be released for reasons of con-

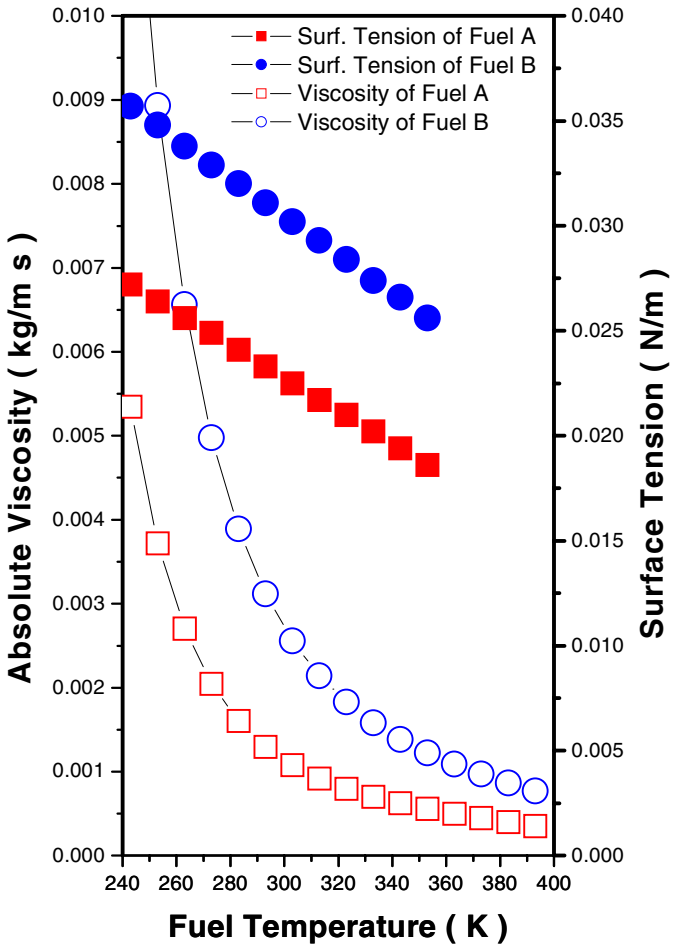

Fig. 5 The variation of the liquid properties (surface tension and dynamic viscosity in the units of [kg/s^2] and [kg/ms], respectively) with the change in the liquid temperature for Fuel A and Fuel B.

fidentiality, the variations of the fuel viscosity and surface tension were experimentally measured and reported in Fig. 5. In Fig. 5, there is a rapid change in viscosity at the near-low-temperature region; the process causes some problematic fuel freezing at low atmospheric temperatures, eventually resulting in poor performance — or no performance — from the pressure-swirl atomizer. The surface tension of the fuel also increases at low temperatures, even though its rate of change is not as abrupt as that of viscosity.

RESULTS AND DISCUSSION

Figure 6 is a series of photographs showing instantaneous fluctuations of the spray at low-temperature conditions. As shown in Fig. 6, the figures differ from each other because of unsteadiness from the pulsation that occurred internally and externally during the fuel's low temperature, T = 274.2 K. This phenomenon is hereafter referred to as "the internal–external unstable regime." This unsteady, transitional behavior of the atomizer is attributed to the eruption of the air core due to the increase of fuel viscosity at its low temperature. See Fig. 5 for the abrupt gradient change in the viscosity of the fuel used. The air core, formed due to strong swirl, comes and goes sporadi-

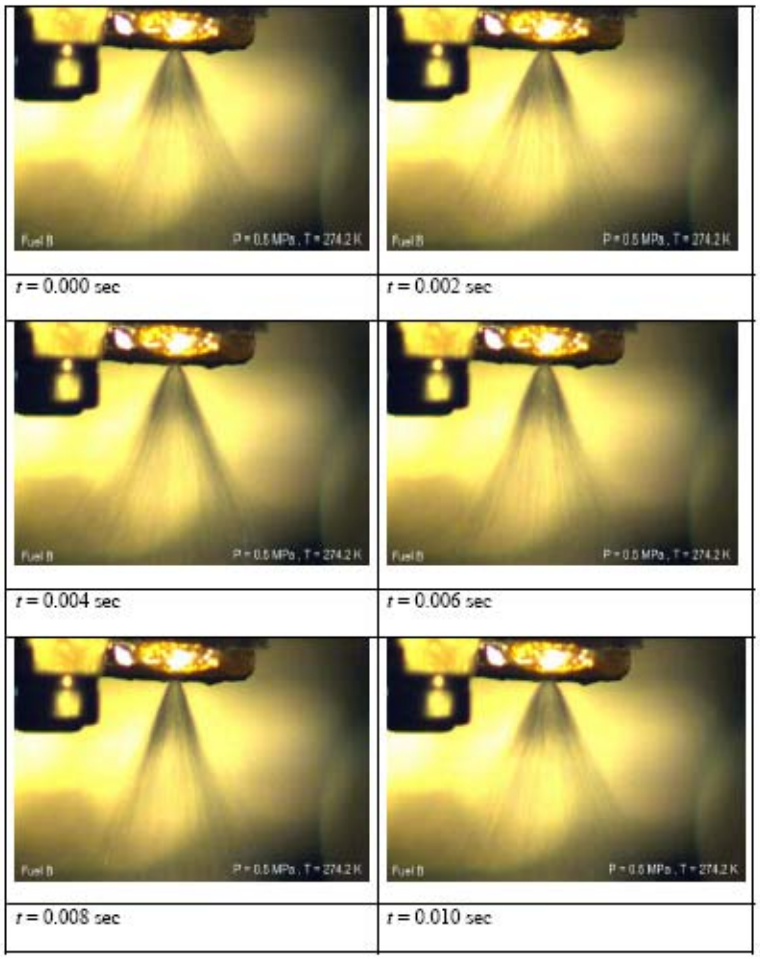

Fig. 6 The time-series plot of the pressure-swirl atomizer during the internal–external unstable regime (Fuel B, T = 274.2 K, P = 0.5 MPa).

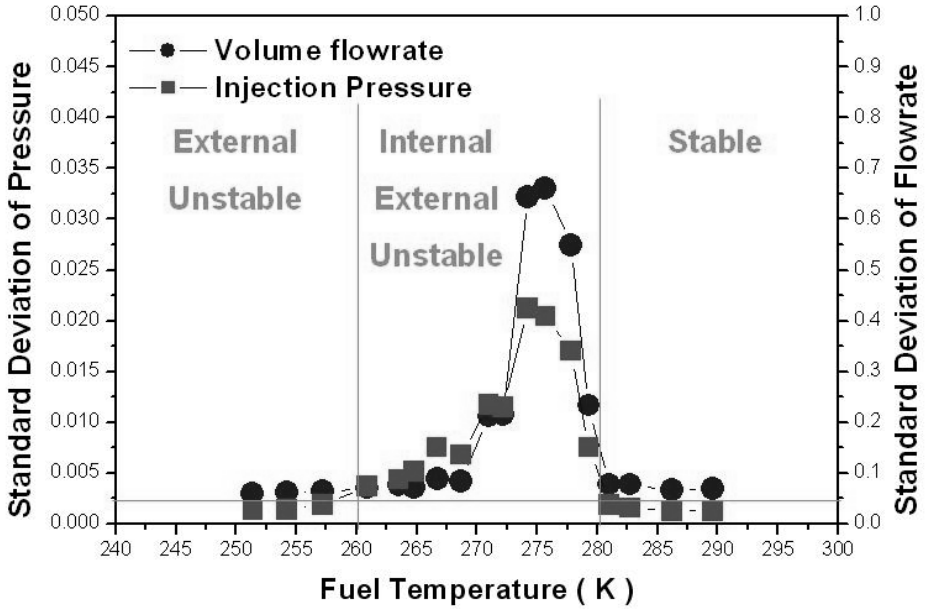

Fig. 7 Standard deviations of the injection pressure and volume flow rate as a function of fuel temperatures.

cally during the internal–external unstable regime, whose range was estimated at approximately 260 K < T < 280 K, according to the standard deviation values of the measured pressure and flow rate shown in Fig. 7.

When the fuel temperature was further reduced (i.e., T < 260 K), the air core completely disappeared since the fuel viscosity dominated the centrifugal force; the swirling strength was not sufficient to maintain the air core at the atomizer's center. In this case, flow becomes unstable inside a pipe due to the thick boundary layer, which induces an adverse pressure gradient. As a result, a turbulent effect starts to appear as an additional source of instability and makes the simplex atomizer unstable omly externally, which is hereafter referred to as "the external unstable regime." Typically, the volumetric distribution of a classic pressure-swirl atomizer follows the hollow-cone distribution. However, the atomizer's volumetric distribution evolves from the hollow-cone to the solid-cone distribution as the atomizer's center is occupied by the entire liquid fuel; no air core is present in the external unstable regime. This distribution evolution is manifest in Fig. 8: The double sharp peaks of the typical hollow-cone distribution, without any droplet mass presence at the center at relatively higher temperature (T = 292.6 K,

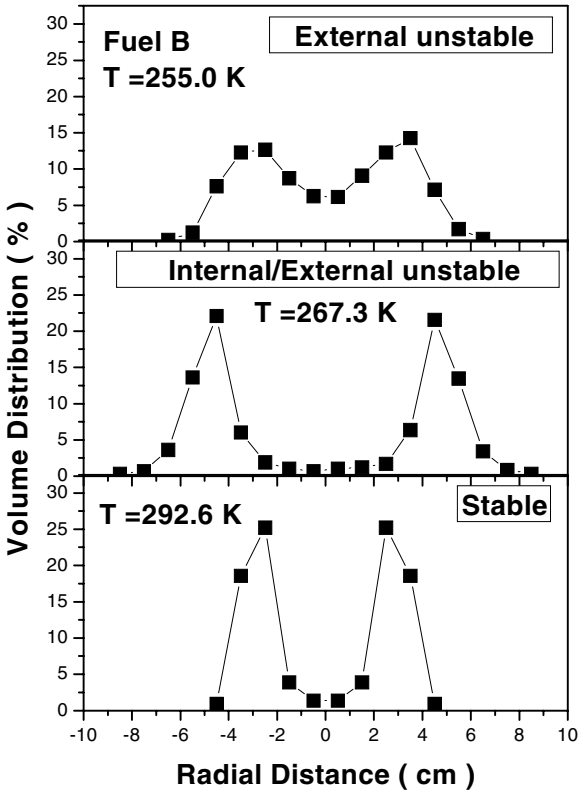

Fig. 8 Volume distribution for the three stability regimes. The liquid used here was Fuel B and the operating pressure was ΔP = 0.5 MPa.

called the "stable" regime"), evolved to a slightly more dispersive distribution during the internal–external unstable region (T = 267.3 K). Eventually, the droplet mass started to fill in the center area when the air core disappeared at T = 255 K. The distribution characteristic has obviously changed from the hollow cone at higher temperatures to the solid cone at lower temperatures, as appears in Fig. 8. It is noteworthy that the helical motion of the internal flow is still maintained as indicated in Fig. 8 (see the case for T = 255 K), despite the disappearance of the air core; two hump shapes remain, which are the characteristic distribution of the hollow-cone atomizer.

Figure 9 shows the measured volumetric flow rate and the operating pressure. The mean volume flow rate for the stable regime is approximately 11.3×10^{-6} m^3/s, while the external unstable regime is around

a)

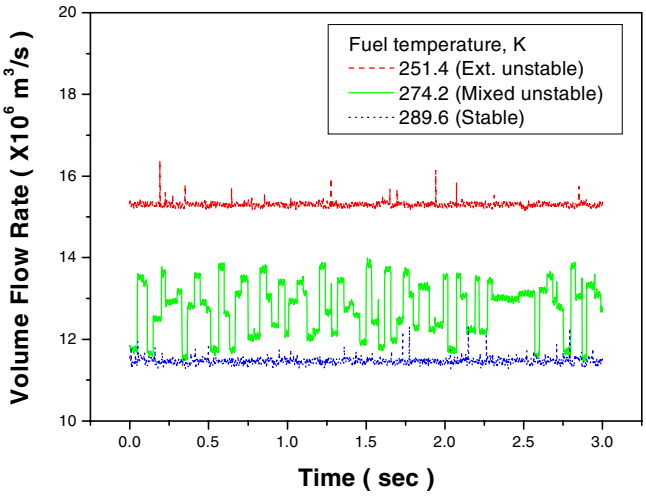

b)

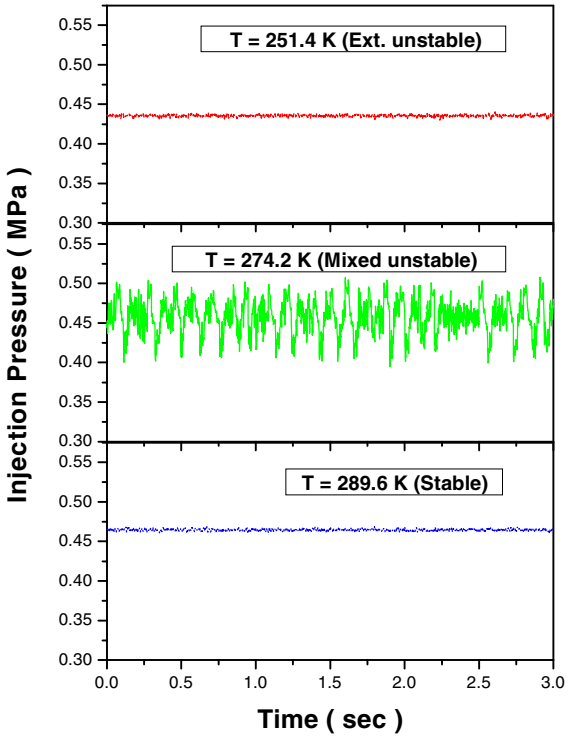

Fig. 9 The histories of (a) the volume flow rate and (b) the injection pressure for the three stability regimes for Fuel B.

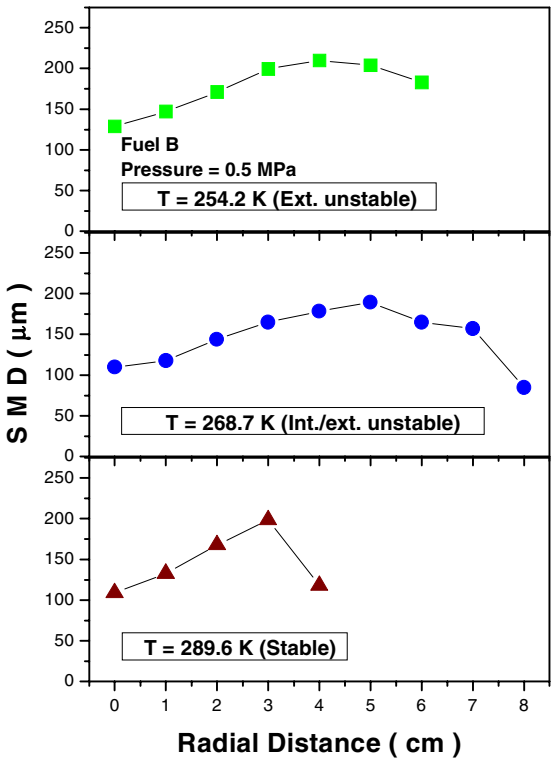

Fig. 10 SMD distribution for the three stability regimes. The operating pressure was ΔP = 0.5 MPa; Fuel B was used.

15.3×10^{-6} m^3/s. This increase in the fuel's flow rate is expected, since the external unstable regime contains no air core and as a result, more cross-sectional area is occupied by the fuel and therefore the higher flow rate. During the internal–external unstable regime, the recorded volumetric flow rate fluctuates severely because of the sporadic formation of the air core. Similar behavior is observed for the recorded pressure; the pressure fluctuates during the internal–external regime even though its mean value remains at ~0.45 MPa ±5%. It must be noted that the slight decrease in the injection pressure in Fig. 9b at lower temperature (external unstable regime) is attributed to the fact that some portion of the total pressure is lost while decreasing the static gage pressure and increasing the dynamic pressure of a higher volumetric flow-rate case, as in Fig. 9a.

The SMD distributions of Fuel B for all three regimes are shown in Fig. 10. All three SMD distributions follow the pattern of up- and downhill,

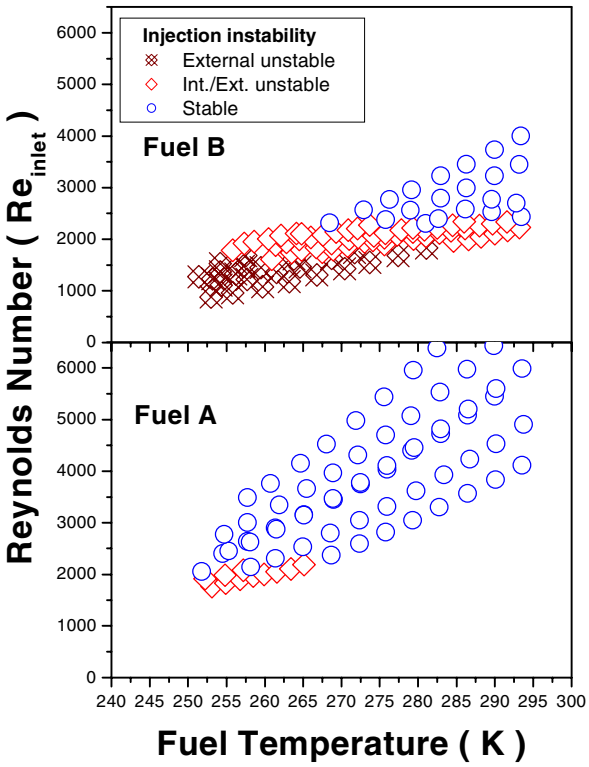

Fig. 11 Stability map for the three stability regimes, represented by the inlet Reynolds number as a function of the fuel temperature.

in an outward direction. The SMD distribution for the internal–external unstable regime covers a wider area due to its severely unstable behavior; the highly fluctuating pressure and flow-rate record are shown in Fig. 7. It is noteworthy that the SMD values tend to be slightly larger with the lower injection temperature (or larger liquid viscosity) because the characteristic eddy size, which affects the SMD value, is known to be proportional to the liquid viscosity [11] during the turbulent regime.

At this point, it is noteworthy that the aforementioned three stability regimes appeared only in Fuel B for the tested range of fuel temperature. For Fuel A, the air core never completely disappeared; only the stable and internal–external unstable regimes were observed, and the external unstable regime was not observed in the tests conducted with Fuel A, as shown in Fig. 11. While deducing the viscosity values of Fuel A and Fuel B, from Fig. 5, at the minimum temperature applied during the test ($T_{\min}$ = 250 K), viscosity

was found to be approximately 0.0045 kg/ms for Fuel A and 0.0100 kg/ms for Fuel B, indicating that viscosity has to be greater than 0.0045 kg/ms (14.5 times greater than the typical viscosity of a gasoline at room temperature) in order to cause the disappearance of the air core. Clearly, the viscosity of Fuel B, 0.0100 kg/ms at $T_{\min} = 250$ K, is unusually high, which result induces poor atomization performance, susceptible to combustion instability.

It should be mentioned that there are two different Reynolds numbers used in this report, as follows. The inlet Reynolds number, $\mathrm{Re}_{\mathrm{inlet}} = U_p D_p/\nu_l$, where $U_p = Q/A$ and $D_p = 1.5$ mm represent the port's inlet velocity and diameter, respectively. A_p is the port cross-sectional area and ν_l is the liquid kinematic viscosity. The volumetric flow rate, Q, is in the unit of [m^3/s]. The subscript for kinematic viscosity, $(\,)_l$, represents the properties of the liquid fuel. Another number is the outlet Reynolds number, defined as $\mathrm{Re} = U_o D_o/\nu_l$, where $U_o = Q/A_o$ and $D_o = 1$ mm represent the orifice (or outlet) velocity and diameter, respectively. Thus, the ratio of the outlet-to-inlet Reynolds number can be expressed with a constant, k, as in $\mathrm{Re} = k\ \mathrm{Re}_{\mathrm{inlet}}$, where $k = D_p/D_o = 1.5$. This ratio indicates that the outlet Reynolds number is 50% larger than the inlet Reynolds number.

The cone angle of the atomizer as a function of the outlet Reynolds number is shown in Fig. 12. As indicated, the cone angle increases when the Reynolds number increases. This pattern is caused by the greater radial component of the liquid-fuel velocity with growing swirling strength when the Reynolds number is increased. The empirical formula for the cone angle of Fuels A and B is provided as $\theta = -31.26 + 20.65 \log_{10}(\mathrm{Re})$, based on the data obtained during the stable regime, because it was difficult to measure the cone angle when the jet was in the unstable regimes of severe fluctuations.

Figure 13 presents the discharge coefficient varying with the outlet Reynolds number. There is a distinct downhill slope within the range of $2500 < \mathrm{Re} < 3500$. This slope is caused by the formation of the air core when the Reynolds number increases. When the air core is formed, the fuel's volumetric, or mass, flow rate, reduces as the center area is occupied by the air core, which is the reason for the reduction in the discharge coefficient. It is clear that this transitional stage occurs with relatively larger fluctuating uncertainty, as shown in Fig. 13. Nevertheless, the collected data fits a reasonable empirical formula, as follows:

$$C_d = 0.57746 + 1.24834 \times 10^{-4}\,\mathrm{Re} - 7.465 \times 10^{-8}\,\mathrm{Re}^2 \quad \text{for} \quad \mathrm{Re} < 3500 \tag{1}$$

$$C_d = 0.31779 + 0.21992 \exp\frac{-\mathrm{Re}}{5603.5142} \quad \text{for} \quad \mathrm{Re} > 3500 \tag{2}$$

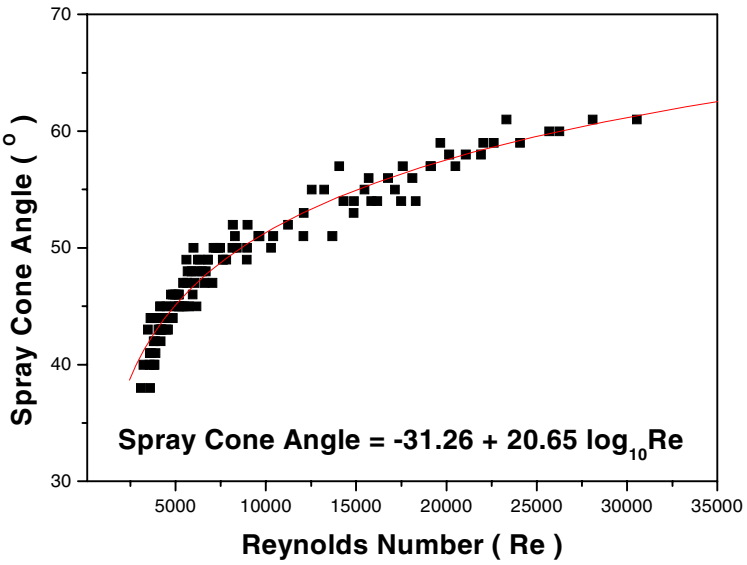

Fig. 12 The variation of the atomizer's cone angle with respect to the outlet Reynolds number varied with the fuel's temperature and the operating pressure, ranging from 0.2 MPa to 1 MPa.

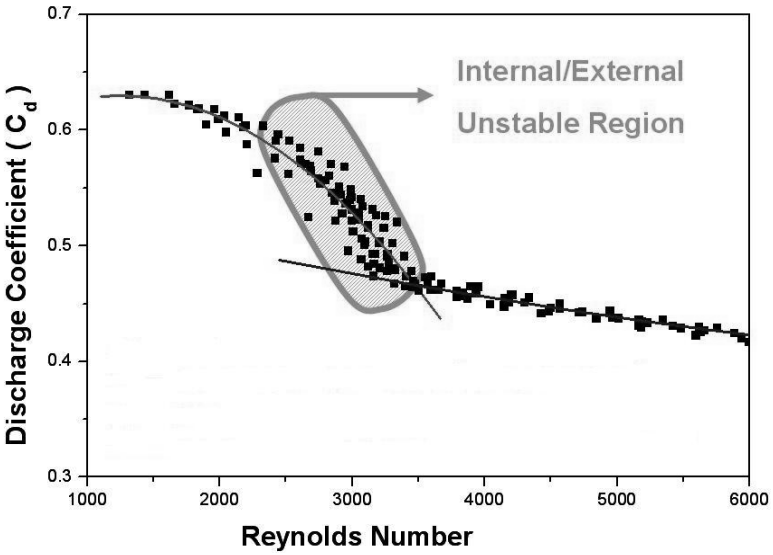

Fig. 13 Discharge coefficient as a function of the outlet Reynolds number. Fuel B was used. The lines are from Eqs. (1) and (2).

CONCLUSIONS

Flow characteristics of a pressure-swirl atomizer were conducted for various fuel temperatures. The working liquid was the kerosene-based fuel type used in aircraft engines. It is shown that the fuel nearly freezes at low atmospheric temperatures, becoming a source for atomizer instabilities. These instabilities were categorized into three different regimes: (1) The external unstable regime, in which the air core disappears due to swirl weakening caused by increased viscosity at low fuel temperatures. Turbulence dominates in this regime and pulsation was observed only externally ($T < 260$ K). (2) The internal–external unstable regime, in which both internal and external flows experienced the transitional stage due to the eruption of the air core during the fuel's viscosity change. The temperature range for this transitional stage was found to be approximately 260 K $< T <$ 280 K. (3) The stable regime is typical of the pressure-swirl atomizer with the air-core column centered vertically throughout the atomizer's internal geometry ($T > 280$ K).

The following recommendations are made to improve the quality of the design for the pressure-swirl atomizer while circumventing the operational limitations associated with cold weather: (1) Orifice length can be reduced to sustain swirling strength, increasing the durability of the air-core existence, (2) Additional ports (or holes) of the tangential entry within the swirling chamber can be added to the swirling strength to maintain the air-core column.

ACKNOWLEDGMENT

This research was supported by a grant R0504532 from Carbon Dioxide Reduction & Sequestration Research Center, one of the 21st Century Frontier Programs funded by the Ministry of Science and Technology of Korean government.

REFERENCES

1. G. I. Taylor, The Mechanics of Swirl Atomizers, *7th Int. Congress of Applied Mechanics*, vol. 2, no. 1, pp. 280–285, 1948.
2. E. Giffen and A. Muraszew, *Atomization of Liquid Fuels*, Chapman & Hall, London, 1953.
3. N. Dombrowski and D Hasson, The Flow Characteristics of swirl Centrifugal Spray Pressure Nozzles with Low Viscosity Liquids, *AIChE J.*, vol. 15, pp. 604–611, 1969.

4. C. J. Clark and N. Dombrowski, Aerodynamic Instability and Disintegration of Inviscid Liquid Sheets, *Proc. R. Soc. London, Ser. A*, vol. 329, pp. 467–478, 1972.
5. N. K. Rizk and A. H. Lefebvre, Internal Flow Characteristics of Simplex Swirl Atomizers, *J. Propul. Power*, vol. 1, no. 3, pp. 193–199, 1985.
6. H. Park and S. D. Heister, Nonlinear Simulation of Free Surfaces and Atomization in Pressure Swirl Atomizers, *Phys. Fluids*, vol. 18, 052103, 2006.
7. A. H. Lefebvre, *Atomization and Sprays*, Hemisphere, Washington, DC, 1983.
8. G. I. Taylor, The Boundary Layer in the Converging Nozzle of a Swirl Atomizer, *Q. J. Mech. Appl. Math.*, vol. 3, no. 2, pp. 129–139, 1950.
9. B. S. Park, H. Y. Kim, Y. C. Kim, and J. T. Chung, An Experimental Study on the Spray Characteristics of a Dual-Orifice Type Swirl Injector at Low Fuel Temperatures, *KSME Int. J.*, vol. 18, no. 7, pp. 1187–1195, 2004.
10. D. Kim, Y. Yoon, and P. Han, Effect of Flow Condition and Geometry on Flow Characteristics of a Swirl Injector, *16th Ann. Conf. Liquid Atomization and Spray Systems*, Monterey, CA, May, 2003.
11. P. K. Wu, L. K. Tseng, and G. M. Faeth, Primary Breakup in Gas/Liquid Mixing Layers for Turbulent Liquids, *Atomization and Sprays*, vol. 2, pp. 295–317, 1992.